BAYESIAN FORMULATION OF SUBBAND AUTOREGRESSIVE MODELLING WITH BOUNDARY CONTINUITY CONSTRAINTS

James R. Hopgood and Peter J. W. Rayner

Signal Processing Laboratory, Department of Engineering,
University of Cambridge, England. CB2 1PZ
jrh1008@eng.cam.ac.uk, pjwr@eng.cam.ac.uk

ABSTRACT

The *all-pole model* is often used to parsimoniously approximate rational transfer functions. In many applications, such as single channel blind deconvolution, an estimate of the channel is required. However, in general, attempting to model the entire channel spectrum by a single all-pole model leads to a large computational load. Hence, it is better to model a particular frequency band of the spectrum by an all-pole model, reducing a single high-dimensional optimistation to a number of low-dimensional ones. If each subband is completely decoupled from the others, and does not enforce any continuity, there will be discontinuities in the spectrum at the subband boundaries. In this paper, continuity is ensured by constraining the subband parameters such that the end points at one subband boundary is matched to the spectrum in the adjacent subbands. This is formulalised in the Bayesian probabilistic framework.

1. SELECTIVE SPECTRAL MODELLING

The *all-pole model* is often used to model a channel since, not only is it mathematically convienient and widely used in many fields, but it often parsimoniously approximates rational transfer functions. This model simultaneously fits the entire frequency range, even though it may fit some regions in this frequency space better than others. For example, acoustic impulse responses (AIRs) may be modelled by a linear time-invariant (LTI) all-pole filter with typical model orders in the range $50 \leq P \leq 500$ [1]. In many applications, such as single channel blind dereverberation [2], an estimate of the AIR is required. However, attempting to model the entire acoustic spectrum by a single all-pole model often leads to a large computational load. Hence, it may be better to model a particular frequency band of the filter's spectrum by an all-pole model. Since the subbands have been decoupled, this often results in a lower model order *for that frequency band* and, therefore, improved parameter estimation within this frequency band. Subband linear prediction has also been considered in [4–6]. Unfortunately, as discussed in [3] where the subband autoregressive (AR) model is applied to room acoustics, since the model in each subband is completely decoupled from the other subbands, there are discontinuities in the model's spectrum at the subband boundaries, which introduce distortion into the equalised channel. The subband model did not enforce any continuity between blocks. In this paper, continuity is ensured by constraining the AR parameters such that the end points at one subband boundary is matched to the estimated spectrum in the adjacent subbands.

This work is supported by William Colton Research Fellowship, Queens' College, University of Cambridge.

2. BAYESIAN FREQUENCY DOMAIN FORMULATION

If a channel is modelled as all-pole excited by white Gaussian noise (WGN), its output, $s(t)$, is given by the AR process:

$$s(t) = -\sum_{p=1}^{P} a(p)\, s(t-p) + e(t), \quad \forall t \in \mathcal{T} \tag{1}$$

where $e(t)$ is the WGN input excitation, $\mathbf{a} = \{a(p),\, p \in \mathcal{P}\}$ are the model parameters, and P is the number of poles. Although the estimate of the autoregressive parameters, $\mathbf{a}$, is usually derived in the time-domain, it can also be formulated within the frequency domain. Makhoul [4] suggests such a formulation when analysing speech using linear prediction. A rigorous Bayesian formulation is derived below, which has previously been summarised in [3].

2.1. Likelihood Function for AR Processes

The sequence $\{s(t),\, t \in \mathcal{T} = \{0, \ldots, T-1\}\}$ is modelled by the AR process given in equation (1). If $e(t) \rightleftharpoons E(k)$ and $s(t) \rightleftharpoons S(k)$ are discrete Fourier transform (DFT) pairs, defined by:

$$S(k) = \frac{1}{\sqrt{T}} \sum_{t=0}^{T-1} s(t)\, e^{-\frac{j2\pi kt}{T}}, s(t) = \frac{1}{\sqrt{T}} \sum_{k=0}^{K-1} S(k)\, e^{\frac{j2\pi kt}{T}}$$

where $k \in \mathcal{K} = \{0, \ldots, K-1\}$ and $t \in \mathcal{T}$, then application of the DFT to (1) for $t \in \mathcal{T}$ gives:

$$E(k) = S(k) + \sum_{p=1}^{P} a(p)\, e^{-\frac{2\pi\, jkp}{T}}\, \hat{S}_p(k) \tag{2}$$

where $\hat{S}_p(k)$ is given by:

$$\hat{S}_p(k) = \frac{1}{T} \sum_{\hat{k}=0}^{K-1} S(\hat{k}) \sum_{t=0}^{T-1-p} e^{\frac{j2\pi(\hat{k}-k)t}{T}} + \underbrace{\frac{1}{\sqrt{T}} \sum_{t=-p}^{-1} s(t) e^{-\frac{j2\pi jt}{T}}}_{\text{initial conditions}}$$

Inclusion of the initial conditions leads to a spectral analogue of the covariance AR modelling method. However, for brevity, the effect of the initial conditions are removed by assuming $s(t)$ is periodic, such that as T gets large, linear convolution can be approximated by circular convolution. In this case, $S(k)$ replaces $\hat{S}_p(k)$ in (2), which can be written in vector-matrix form by defining the vector[1] $[\boldsymbol{\mathcal{E}}]_k = E(k),\, k \in \mathcal{K}$:

$$\boldsymbol{\mathcal{E}} = \boldsymbol{\mathcal{S}} + \mathbf{S}\,\mathbf{a} \tag{3}$$

[1] In addition to bold lower case letters, bold calligraphic letters are used to denote vectors. Bold capital letters denote matrices.

where $\mathbf{S} = [\boldsymbol{\mathcal{S}}_1 \ \cdots \ \boldsymbol{\mathcal{S}}_P]$, $[\boldsymbol{\mathcal{S}}_p]_k = e^{-\frac{2\pi jkp}{T}} S(k), k \in \mathcal{K}$, and $\boldsymbol{\mathcal{S}} = \boldsymbol{\mathcal{S}}_0$. Defining $[\mathbf{W}_T]_{k,t} \triangleq \frac{1}{\sqrt{T}} e^{-\frac{2\pi jkt}{T}}$, $k \in \mathcal{K}$, $t \in \mathcal{T}$, then $\boldsymbol{\mathcal{E}} = \mathbf{W}_T\, \mathbf{e}$, where $[\mathbf{e}]_t = e(t)$, $t \in \mathcal{T}$ and $\mathbf{e} \sim \mathcal{N}\left(\mathbf{0}_T,\, \sigma^2\, \mathbf{I}_T\right)$; $\mathbf{I}_T \in \mathbb{R}^{T\times T}$ is the identity. Next, assume T is even,[2] and observe $E(k) = E^*(T-k)$, $k \in \hat{\mathcal{K}} = \{1, \ldots, \hat{K}\}$ where $\hat{K} = \frac{T}{2} - 1$, and that $E(0)$ and $E\left(\frac{T}{2}\right)$ are real. Defining the new random variables (r. v.s) $E_r(k) = \Re\{E(k)\}$, $k \in \tilde{\mathcal{K}} = \{0, \ldots, \tilde{K}\}$, $\tilde{K} = \frac{T}{2}$ and $E_i(k) = \Im\{E(k)\}$, $k \in \hat{\mathcal{K}}$, where $\Re\{\cdot\}$ and $\Im\{\cdot\}$ denote the real and imaginary components respectively, yields a real mapping from T real r. v.s in $\mathbf{e}$ to T real r. v.s in $\hat{\boldsymbol{\mathcal{E}}} = \{E_r(k),\, k \in \tilde{\mathcal{K}},\, E_i(k),\, k \in \hat{\mathcal{K}}\}$. From the definition of the DFT, it follows:

$$\underbrace{\begin{bmatrix} E_r(0) \\ \vdots \\ E_r(\tilde{K}) \\ E_i(1) \\ \vdots \\ E_i(\hat{K}) \end{bmatrix}}_{\hat{\boldsymbol{\mathcal{E}}}} = \underbrace{\begin{bmatrix} c_{0,0} & \cdots & c_{0,T-1} \\ \vdots & \ddots & \vdots \\ c_{\tilde{K},0} & \cdots & c_{\tilde{K},T-1} \\ s_{0,0} & \cdots & s_{0,T-1} \\ \vdots & \ddots & \vdots \\ s_{\hat{K},0} & \cdots & s_{\hat{K},T-1} \end{bmatrix}}_{\hat{\mathbf{W}}_T} \underbrace{\begin{bmatrix} e(0) \\ \vdots \\ e(\tilde{K}) \\ e(\tilde{K}+1) \\ \vdots \\ e(T-1) \end{bmatrix}}_{\mathbf{e}} \tag{4}$$

where $c_{k,t} = \frac{1}{\sqrt{T}} \cos\left(\frac{2\pi kt}{T}\right)$ and $s_{k,t} = -\frac{1}{\sqrt{T}} \sin\left(\frac{2\pi kt}{T}\right)$. Using the probability transformation rule, where if $\mathbf{y} = \mathrm{A}\,\mathbf{x}$, then:

$$p_y(\mathbf{y}) = \frac{1}{\mathrm{abs}\,|\mathrm{A}|} p_x\left(\mathrm{A}^{-1}\,\mathbf{y}\right) \tag{5}$$

and noting $\mathbf{e} \sim \mathcal{N}\left(\mathbf{0}_T,\, \sigma^2\, \mathbf{I}_T\right)$, it follows:

$$p_{\hat{\mathcal{E}}}\left(\hat{\boldsymbol{\mathcal{E}}}\right) = \mathcal{N}\left(\hat{\boldsymbol{\mathcal{E}}} \,|\, 0,\, \sigma^2\, \hat{\mathbf{W}}_T\, \hat{\mathbf{W}}_T^T\right) \tag{6}$$

From the definition of $\hat{\mathbf{W}}_T$, it may be shown that

$$\left[\hat{\mathbf{W}}_T\, \hat{\mathbf{W}}_T^T\right]_{k,\hat{k}} = \begin{cases} 1 & \text{if } k = \hat{k} = 0, \text{ or } k = \hat{k} = \frac{T}{2} \\ \frac{1}{2} & \text{if } k = \hat{k} \neq 0, \text{ or } k = \hat{k} \neq \frac{T}{2} \\ 0 & \text{otherwise} \end{cases} \tag{7}$$

It follows $\hat{\boldsymbol{\mathcal{E}}}^T \left(\hat{\mathbf{W}}_T \hat{\mathbf{W}}_T^T\right)^{-1} \hat{\boldsymbol{\mathcal{E}}} =$

$$E_r^2(0) + E_r^2\left(\tfrac{T}{2}\right) + 2\sum_{k=1}^{\hat{K}} \left\{E_r^2(k) + E_i^2(k)\right\} \equiv \boldsymbol{\mathcal{E}}^\dagger\, \boldsymbol{\mathcal{E}}$$

where the equivalence comes from simply expanding $\boldsymbol{\mathcal{E}}^\dagger\, \boldsymbol{\mathcal{E}}$. Hence:

$$p_{\mathcal{E}}\left(\boldsymbol{\mathcal{E}}\right) \propto \mathcal{N}\left(\boldsymbol{\mathcal{E}} \,|\, 0,\, \sigma^2\, \mathbf{I}_T\right) \tag{8}$$

as expected since, by Parseval's Theorem in finite-discrete time $\mathbf{e}^T\, \mathbf{e} = \boldsymbol{\mathcal{E}}^\dagger\, \boldsymbol{\mathcal{E}}$, noting $\mathbf{W}_T^\dagger \mathbf{W}_T = \mathbf{I}_T$. Using (5) again, the likelihood function is:

$$p_{\mathcal{S}}\left(\boldsymbol{\mathcal{S}} \mid \boldsymbol{\theta}, \mathcal{I}\right) \propto \frac{1}{\left(2\pi\sigma^2\right)^{\frac{T}{2}}} \exp\left\{-\frac{\|\boldsymbol{\mathcal{S}} + \mathbf{S}\,\mathbf{a}\|^2}{2\sigma^2}\right\} \tag{9}$$

where $\|\cdot\|$ denotes the Euclidean norm, $\boldsymbol{\theta} = \{\mathbf{a}, \sigma^2\}$ are the model parameters, and $\mathcal{I}$ denotes the underlying models used. The *posterior probability*, $p\left(\boldsymbol{\theta} \mid \boldsymbol{\mathcal{S}}, \mathcal{I}\right)$, is given by Bayes's theorem:

$$p\left(\boldsymbol{\theta} \mid \boldsymbol{\mathcal{S}}, \mathcal{I}\right) \propto p\left(\boldsymbol{\mathcal{S}} \mid \boldsymbol{\theta}, \mathcal{I}\right)\, p\left(\boldsymbol{\theta} \mid \mathcal{I}\right) \tag{10}$$

where $p\left(\boldsymbol{\theta} \mid \mathcal{I}\right)$ represents any prior belief.

[2] The derivation is similar if T is odd.

2.2. Prior distribution on AR coefficients

For a real, stable, minimum-phase AR process, $\mathbf{a}$, should ideally only take on values which lie in the *stability domain*. However, it is usual to place a Gaussian prior on the parameters: $\mathbf{a} \,|\, \sigma^2 \sim \mathcal{N}\left(\mathbf{0}_P,\, \sigma^2\, \delta^2\, \mathbf{I}_P\right)$, $\delta \in \mathbb{R}^+$.

2.3. Prior distribution for the Excitation Variance

A standard prior for scale parameters, such as variances, is the inverse-Gamma density: $p\left(\sigma^2 \,\middle|\, \alpha, \beta\right) = \mathcal{IG}\left(\sigma^2 \,\middle|\, \frac{\alpha}{2},\, \frac{\beta}{2}\right)$,

$$\mathcal{IG}\left(\sigma^2 \,|\, \alpha,\, \beta\right) = \frac{\beta^\alpha (\sigma^2)^{-(\alpha+1)}}{\Gamma(\alpha)} \exp\left(-\frac{\beta}{\sigma^2}\right) \mathbb{I}_{\mathbb{R}^+}\left(\sigma^2\right)$$

where $\mathbb{I}_{\mathcal{A}}(a) = 1$ if $a \in \mathcal{A}$ and zero otherwise.

2.4. Parametric Estimate of AR Coefficients

The hyperparameters $\{\alpha,\, \beta,\, \delta\}$ are, for simplicity, assumed to be known. From (9) and (10), the joint density is:

$$p\left(\boldsymbol{\theta} \mid \boldsymbol{\mathcal{S}}, \mathcal{I}\right) \propto \frac{1}{\sigma^R} \exp\left\{-\frac{\|\boldsymbol{\mathcal{S}} + \mathbf{S}\,\mathbf{a}\|^2 + \frac{1}{\delta}\mathbf{a}^T\mathbf{a} + \beta}{2\sigma^2}\right\} \tag{11}$$

where $R = T + P + \alpha + 2$. This can be maximised with respect to $\mathbf{a}$ and σ, yielding the maximum marginal *a posteriori* (MMAP) solution, which is similar to the usual least-squares solution:

$$\begin{aligned} \hat{\mathbf{a}} &= -\left(\mathbf{S}^\dagger\mathbf{S} + \delta^{-2}\right)^{-1} \Re\left\{\mathbf{S}^\dagger\, \boldsymbol{\mathcal{S}}\right\} \\ \hat{\sigma}^2 &= R^{-1}\left(\boldsymbol{\mathcal{S}}^\dagger\, \boldsymbol{\mathcal{S}} + \Re\left\{\boldsymbol{\mathcal{S}}^\dagger\, \mathbf{S}\,\mathbf{a}\right\} + \beta\right) \end{aligned} \tag{12}$$

3. BAYESIAN SUBBAND MODELLING

The Bayesian analysis above can be extended to model an observed process in subbands, rather than a single "full-band". In each subband, the power spectrum, $\mathcal{P}(k) = \mathbb{E}\left\{|S(k)|^2\right\}$, of $s(t)$ is modelled by an all-pole spectrum in the region $k \in \mathcal{K}_l = \{k_l, \ldots, k_{l+1} - 1\}$, where l denotes the subband index, $T_l \equiv K_l = k_{l+1} - k_l$ is the number of frequency components in band $l \in \mathcal{L} = \{0, \ldots, L-1\}$, L is the number of subbands, $\boldsymbol{\omega} = \{k_l,\, l \in \mathcal{L}\}$ are the subband boundaries, $k_0 \triangleq 0$ and $k_L \triangleq T$. In other words, considering (2), $\mathcal{P}(k)$ can be represented over the full frequency range by a series of subband models, as given by:

$$\mathbb{E}\left\{|S(k)|^2\right\} = \sum_{l=0}^{L-1} \frac{\sigma_l^2\, \mathbb{I}_{\{k_l, k_{l+1}\}}(\omega)}{\left|1 + \sum_{p=1}^{P_l} a_l(p)\, e^{-\frac{2\pi\, j(k-k_l)p}{k_{l+1}-k_l}}\right|^2} \tag{13}$$

where $\mathbf{a}_l = \{a_l(p),\, p \in \mathcal{P}_l\}$ and σ_l^2 denote model parameters in subband l. The spectral error, $\boldsymbol{\mathcal{E}} = \mathbf{W}_T\, \mathbf{e}$, is divided into subbands, $\boldsymbol{\mathcal{E}} = [\boldsymbol{\mathcal{E}}_0, \ldots, \boldsymbol{\mathcal{E}}_{\{L-1\}}]^T$. The variance within each subband, σ_l^2, can be made independent, provided the total power remains constant; *i.e.* $\sum_{l=0}^{L-1} \sigma_l^2 = \sigma^2$. Hence, (8) becomes:

$$p_{\mathcal{E}}\left(\boldsymbol{\mathcal{E}}\right) \propto \prod_{l=0}^{L-1} \mathcal{N}\left(\boldsymbol{\mathcal{E}}_l \,|\, 0,\, \sigma_l^2\, \mathbf{I}_{T_l}\right) \tag{14a}$$

where $\sum_{l=0}^{L-1} T_l = T$. It follows, in analogy to (3):

$$\boldsymbol{\mathcal{E}}_l = \boldsymbol{\mathcal{S}}_l + \mathbf{S}_l\, \mathbf{a}_l \tag{14b}$$

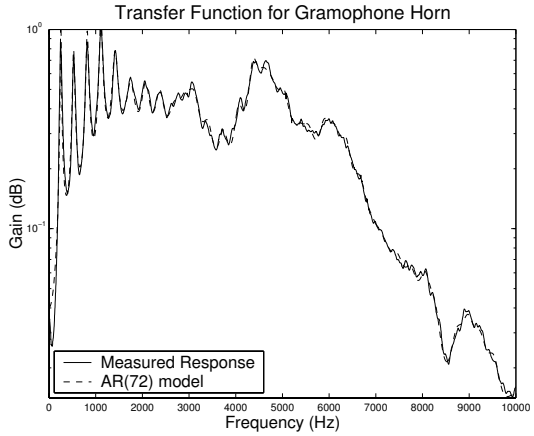

Fig. 1. The transfer function of the horn, and the corresponding AR model; Response, $0 \rightarrow 10\,\text{kHz}$.

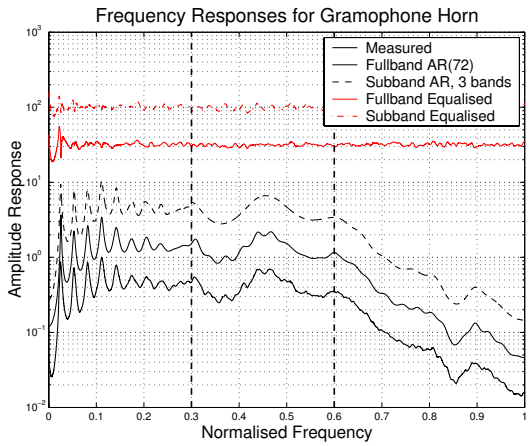

Fig. 2. Modelling the transfer function in Figure 1 using three subbands. The vertical lines denotes the subband boundary.

Denoting $\boldsymbol{\theta} = \{\mathbf{a}_l,\, \sigma_l^2,\, l \in \mathcal{L}\}$, the likelihood is:

$$p\left(\boldsymbol{\mathcal{S}} \mid \boldsymbol{\theta},\, \boldsymbol{\phi},\, \mathcal{I}\right) = \prod_{l=0}^{L-1} \frac{1}{\left(2\pi\sigma_l^2\right)^{\frac{T_l}{2}}} \exp\left\{-\frac{\|\boldsymbol{\mathcal{S}}_l + \mathbf{S}_l\,\mathbf{a}_l\|^2}{2\sigma_l^2}\right\} \tag{15}$$

where $\boldsymbol{\phi} \triangleq \{\boldsymbol{\omega},\, \boldsymbol{\Xi}\}$ contains the vector of subband boundaries, $\boldsymbol{\omega}$, and the vector of model orders, $\boldsymbol{\Xi} = \{P_l,\, l \in \mathcal{L}\}$. The priors attributed to $\mathbf{a}_l$ and σ_l^2 are again $\mathbf{a}_l \mid \sigma_l^2 \sim \mathcal{N}\left(\mathbf{0}_{P_l},\, \sigma_l^2\,\delta_l^2\,\mathbf{I}_{P_l}\right)$, $\delta_l \in \mathbb{R}^+$ and $\sigma_l^2 \mid \left(\frac{\nu_l}{2},\, \frac{\gamma_l}{2}\right) \sim \mathcal{IG}\left(\frac{\nu_l}{2},\, \frac{\gamma_l}{2}\right)$, where $\{\delta_l,\, \nu_l,\, \gamma_l,\, l \in \mathcal{L}\}$ are assumed known. Bayes's theorem gives $p\left(\boldsymbol{\theta} \mid \boldsymbol{\mathcal{S}},\, \boldsymbol{\phi},\, \mathcal{I}\right)$, with the joint density given by the product of terms similar to that in (11), yielding the MMAP solution:

$$\begin{aligned} \hat{\mathbf{a}}_l &= -\left(\mathbf{S}_l^\dagger \mathbf{S}_l + \delta_l^{-2}\right)^{-1} \Re\left\{\mathbf{S}_l^\dagger\, \boldsymbol{\mathcal{S}}_l\right\} \\ \hat{\sigma}_l^2 &= \frac{\boldsymbol{\mathcal{S}}_l^\dagger\, \boldsymbol{\mathcal{S}}_l + \Re\left\{\boldsymbol{\mathcal{S}}_l^\dagger\, \mathbf{S}_l\, \mathbf{a}_l\right\} + \beta_l}{T_l + P_l + \alpha_l + 2} \end{aligned} \tag{16}$$

3.1. Subband Modelling Examples

As a typical channel, consider the frequency response of an acoustic gramophone horn as measured in [7]. The magnitude response is shown in Figure 1, and using a maximum-likelihood estimator for model selection, Spencer [7] shows that this response can be accurately modelled by a 72th-order all-pole model, depending on the model selection estimator. This response is modelled with multiple subbands which, together, span the full frequency range. The *subband model orders*, *changepoint* locations, and the *number of subbands* must be chosen. These can be built into a general model and their values estimated by sampling the joint posterior distribution for all these variables using MCMC methods. Here, the number of subbands and their locations are chosen to be uniformally distributed across the full frequency range. Since the data is being fitted by an AR model, each subband model order is selected using Akaike's B-Information Criterion (BIC), which gives approximately the same solution as if the joint pdf of the AR parameters and model order were maximised. Figure 2 shows[3] that, for the case when $L = 3$, the fit to the original response is just as accurate as the full-band model, but only needs 51 parameters. The individual subband models, as indicated by Table 1, are smaller, $\boldsymbol{\Xi} = \{32, 6, 13\}$, and consequently easier to manipulate. However, since there are no boundary constraints, discountinuities are present, as shown in Figure 3, where 10 subbands are used.

[3] In each figure, the different responses are offset to improve clarity.

L	*Subband Boundaries*; $\frac{\omega}{\pi}$	*Subband Model Orders*; $\boldsymbol{\Xi}$	$\sum P_l$
1	–	72	72
3	$\{0.3,\, 0.6\}$	$\{32, 6, 13\}$	51
10	$\{0.1, 0.2, \ldots, 0.9\}$	$\{18, 8, 2, 2, 2, 4, 5, 1, 5, 2\}$	49

Table 1. Summary of the number of subbands, subband boundaries, subband model orders, and the total number of parameters.

4. SUBBAND BOUNDARY CONSTRAINTS

In this section, the parameters are constrained to ensure continuity across subbands. From (13), if $k = k_{l+1} + \delta k$, then as $\delta k \rightarrow 0$:

$$\mathbb{E}\left\{|S(k)|^2\right\} \rightarrow \frac{\sigma_{l+1}^2}{\left|1 + \sum_{p=1}^{P_{l+1}} a_{l+1}(p)\right|^2} \tag{17a}$$

If $k = k_{l+1} - \delta k$, where $\delta k \rightarrow 0$, then

$$\mathbb{E}\left\{|S(k)|^2\right\} \rightarrow \frac{\sigma_l^2}{\left|1 + \sum_{p=1}^{P_l} (-1)^p\, a_l(p)\right|^2} \tag{17b}$$

Equating these leads to the relationship, for $l \geq 2$:

$$a_l(P_l) = -1 + \sqrt{T_l}\sigma_l\alpha_{l-1} - \textstyle\sum_{p=1}^{P_l-1} a_l(p) \tag{18a}$$

where $$\alpha_l = \pm\frac{1}{\sqrt{T_l}\sigma_l}\left(1 + \textstyle\sum_{p=1}^{P_l}(-1)^p\, a_l(p)\right)$$

Hence: $$\mathbf{a}_l = \mathbf{u}_l + \sqrt{T_l}\sigma_l\,\boldsymbol{\alpha}_l + \mathbf{F}_l\,\hat{\mathbf{a}}_l,\ l \geq 2 \tag{18b}$$

where $\hat{\mathbf{a}}_l \in \mathbb{R}^{P_l-1}$ is the new reduced parameter vector, $\mathbf{u}_l^T = [\mathbf{0}_{P_l-1}^T, -1]$, $\boldsymbol{\alpha}_l = \alpha_{l-1}\,\mathbf{u}_l$, and $\mathbf{F}_l^T = [\mathbf{I}_{P_l-1}, -\mathbf{1}_{P_l-1}]$, $\mathbf{1}_P \in \mathbb{R}^P$ is the vector of 1's. Dropping the subscripts for clarity, then substituting (18b) into (14b) gives:

$$\boldsymbol{\mathcal{E}} = \hat{\boldsymbol{\mathcal{S}}} + \sqrt{T}\sigma\,\hat{\boldsymbol{\alpha}} + \hat{\mathbf{S}}\,\hat{\mathbf{a}} \tag{19}$$

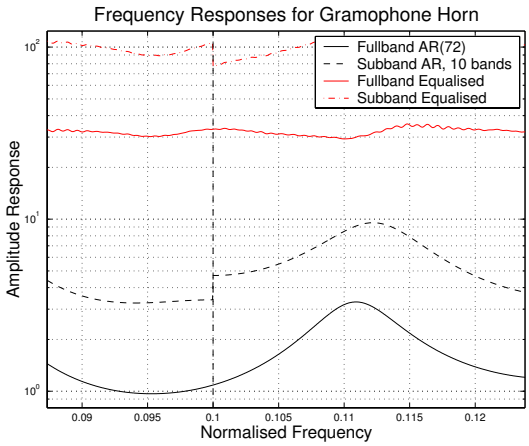

Fig. 3. Modelling the transfer function in Figure 1 using 10 subbands, showing the discontinuities at the subband boundaries.

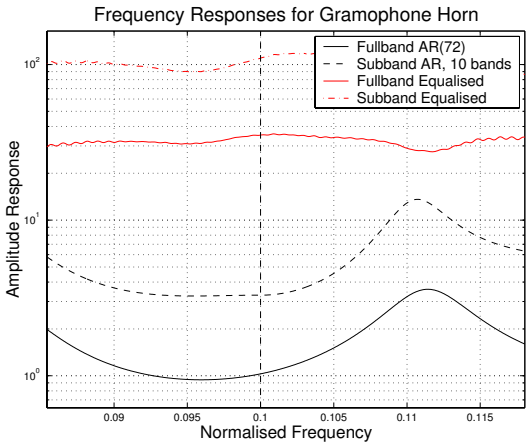

Fig. 4. Modelling the transfer function in Figure 1 using 10 subbands, with the continuity constraint.

where $\hat{\boldsymbol{\mathcal{S}}} = \boldsymbol{\mathcal{S}} + \mathbf{S}\,\mathbf{u}$, $\hat{\boldsymbol{\alpha}} = \mathbf{S}\,\boldsymbol{\alpha}$, and $\hat{\mathbf{S}} = \mathbf{S}\,\mathbf{F}$. The spectral error term is now a function of the parameters in adjacent subbands, and consequently, a full Bayesian analysis should take this into account. However, the likelihood function of (15) soon becomes analytically intractable. Hence, as an approximation, the subband parameters in subband l, $\mathbf{a}_l$, are calculated *independently* of the other subband parameters, not *jointly*, which would be more accurate. Differentiating the log-likelihood term:

$$\ln\left\{\frac{1}{(2\pi\sigma^2)^{\frac{T}{2}}}\exp\left(-\frac{\boldsymbol{\mathcal{E}}^\dagger\boldsymbol{\mathcal{E}}}{2\sigma^2}\right)\right\}$$

with respect to $\mathbf{a}$ and σ leads to the solutions:

$$\hat{\mathbf{a}} = \underbrace{[-(\hat{\mathbf{S}}^\dagger\hat{\mathbf{S}})^{-1}\hat{\mathbf{S}}^\dagger\hat{\boldsymbol{\mathcal{S}}}]}_{\mathbf{a}_1} + \sqrt{T}\sigma\underbrace{[-\hat{\mathbf{S}}^\dagger\hat{\mathbf{S}})^{-1}\hat{\mathbf{S}}^\dagger\hat{\boldsymbol{\alpha}}]}_{\mathbf{a}_2} \qquad (20)$$

where it is noted that $\mathbf{a}_1$ is the least-squares solution without any boundary constraints, and since $\sigma \neq 0$, σ is the solution to:

$$\begin{aligned} E_1^2 + 2\sqrt{T}\sigma\left(\hat{\boldsymbol{\mathcal{S}}} + \hat{\mathbf{S}}\,\mathbf{a}_1\right)^\dagger\left(\tfrac{1}{2}\hat{\boldsymbol{\alpha}} + \hat{\mathbf{S}}\,\mathbf{a}_2\right) \\ + T\sigma^2\left[\mathbf{a}_2^\dagger\hat{\mathbf{S}}^\dagger\left(\hat{\boldsymbol{\alpha}} + \hat{\mathbf{S}}\,\mathbf{a}_2\right) - 1\right] = 0 \end{aligned} \qquad (21)$$

where $E_1^2 = \|\hat{\boldsymbol{\mathcal{S}}} + \hat{\mathbf{S}}\,\mathbf{a}_1\|^2 = \hat{\boldsymbol{\mathcal{S}}}^\dagger[\mathbf{I}_T - \hat{\mathbf{S}}(\hat{\mathbf{S}}^\dagger\hat{\mathbf{S}})^{-1}\hat{\mathbf{S}}^\dagger]\hat{\boldsymbol{\mathcal{S}}}$. The appropriate solution to (20) and (21) is chosen to minimise the overall modelling error. Note that since the estimation is not performed jointly, the current implementation is not symmetrical, since a subband is constrained only by the subband to the left, not to the right. This lack of symmetry can almost be removed by iteratively estimating the subband coefficients by sweeping from subband 1 to L, and then in the reverse direction, with the constraint using the right-hand subband. Details of this will be published elsewhere.

4.1. Subband Modelling Examples

To show the improvement using this method, the response in Figure 1 is again modelled using 10 subbands with continuity constraints. Although not shown, the fit to the original response is very accurate and, as shown in Figure 4, the equalised response is smoother and the discontinuities are removed. The penalty, however, is that the total number of required parameters has risen from $\sum P_l = 49$ to $\sum P_l = 76$, which is larger than the full-band model order $P = 72$. Nevertheless, since individual subband model orders are small, overall, the computational load is reduced.

5. CONCLUSIONS

Subband modelling of AR processes, as described in [3], introduces distortion in the modelled response since each subband is decoupled from the others, thereby inducing discontinuities at the subband boundaries. Continuity constraints have been incorporated in the estimation of the model parameters, thereby reducing the effect of these discontinuities. This reduces distortion in the equalised response, and is extremely useful for audio restoration, where these distortions would be audible. Moreover, the constrained subband model still achieves the objective of reducing a high-dimensional optimisation problem to a number of low-dimensional ones in applications which demand channel estimates.

6. REFERENCES

[1] J. N. Mourjopoulos and M. A. Paraskevas, "Pole and zero modeling of room transfer functions," *Journal of Sound and Vibration*, vol. 146, no. 2, pp. 281 – 302, Apr. 1991.

[2] J. R. Hopgood and P. J. W. Rayner, "Bayesian single channel blind deconvolution using parametric signal and channel models," in *Proc. IEEE WASPAA*, Mohonk, Oct. 1999, pp. 151 – 154.

[3] J. R. Hopgood and P. J. W. Rayner, "A probabilistic framework for subband autoregressive models applied to room acoustics," in *11th Proc. IEEE SSP*, Aug. 2001, pp. 492 – 494.

[4] J. Makhoul, "Spectral analysis of speech by linear prediction," *IEEE Trans. Audio and Electro.*, vol. AU-21, no. 3, pp. 140–148, June 1973.

[5] S. L. Tan and T. R. Fischer, "Linear prediction of subband signals," *IEEE J. Sel. Areas Comms.*, vol. 12, no. 9, pp. 1576–1583, Dec. 1994.

[6] S. Rao and W. A. Pearlman, "Analysis of linear prediction, coding, and spectral estimation from subbands," *IEEE Trans. Information Theory*, vol. 42, no. 4, pp. 1160–1178, July 1996.

[7] P. S. Spencer, *System Identification with Application to the Restoration of Archived Gramophone Recordings*, Ph. D. Thesis, University of Cambridge, UK, June 1990.